Solid-state electronic conductivity of ruthenium nanoparticles passivated by metal–carbon covalent bonds

Debraj Ghosh, Shaowei Chen *

Department of Chemistry and Biochemistry, University of California, Santa Cruz, CA 95064, United States

ARTICLE INFO

ABSTRACT

Stable ruthenium nanoparticles were prepared by passivation of the metal cores (diameter 2.7–3.2 nm by transmission electron microscopy) with ruthenium–carbon covalent bonds. Electrochemical study showed that the electronic conductivity of the particle films exhibited metal-like temperature dependence, and it decayed exponentially with the length of the alkyl spacer of the aliphatic protecting ligands, with an electronic coupling coefficient (β) of 0.48 Å^{-1}. This was ascribed to the strong Ru–C bonding interaction and low interfacial contact resistance where the spilling of core electrons into the organic protecting shell led to enhanced interparticle charge transfer.

1. Introduction

Nanosized metal and semiconductor particles have attracted intense research interest due to their unique chemical and physical properties which differ greatly from those of their constituent atoms/molecules and bulk forms [1]. Of these, monolayer protected clusters (MPCs) represent a unique set of nanomaterials, where the electronic conductivity can be readily manipulated by the inorganic cores as well as the organic protecting shell. Previously thiol derivatives have been used as the ligand of choice in the preparation of many of these MPCs by virtue of the strong metal–sulphur bond. However, because of its lack of interesting chemistry, the effect of the interfacial bonding interaction on the particle electronic conductivity has been largely ignored and unexplored. Recently, with the emergence of new chemistry in the stabilization of metal nanoparticles by metal–carbon covalent bonds [2–5], very unusual conductivity properties have been observed. This is attributed to the enhanced metal–ligand bonding interactions and hence diminishment of interfacial resistance, leading to extended spilling of core electrons into the organic protecting layer. For instance, we recently prepared a series of palladium nanoparticles passivated by Pd–C covalent bonds by the reduction of diazonium derivatives [2], which exhibited electronic conductivity a few orders of magnitude greater than that of the alkanethiolate-protected counterparts (of similar core size and comparable length of the alkyl segment). More significantly, with a short alkyl spacer in the particle protecting ligands, the Pd–C particles displayed metallic temperature dependence of the solid-state conductivity; whereas with a longer alkyl spacer, a metal-to-semiconductor transition was clearly manifested at *ca.* 200 K, which was accounted for by the Mott's metal-insulator

transition model. Similar behaviors were observed with titanium nanoparticles passivated by Ti–C covalent bonds [3]. In a more recent study where ruthenium nanoparticles were prepared by the stabilization of ruthenium–carbene π bonds [6], nanoparticle-mediated intervalence transfer was observed with redox-active moieties that were covalently bound onto the nanoparticle surface through a conjugated linkage. This further illustrates the fundamental impacts of metal–ligand bonding interactions on intraparticle charge delocalization.

In this study, we report the synthesis of ruthenium nanoparticle passivated by ruthenium–carbon single bonds and electrochemical evaluation of the electronic conductivity of the particle solid films. Experimentally, the length of the alkyl segment in the particle protecting ligands was systematically varied and the effect on the particle electronic conductivity was carefully examined and compared. The motivation is primarily two folds. First, because of the significantly stronger Ru–C bond (616.2 kJ/mol) than the Pd–C (436 kJ/mol) and Ti–C (423 kJ/mol) bonds [7], the electronic conductivity of the Ru–C nanoparticles is anticipated to be far greater than that of the Pd–C and Ti–C counterparts, and hence a more prominent metallic character within the same temperature range. Second, as interparticle charge transfer is facilitated by the extended spilling of core electrons into the organic protecting layer, the electronic coupling coefficient (β) is anticipated to be substantially smaller than that in the presence of a more localized metal–ligand bonding contact (e.g., metal–sulphur bonds).

2. Experimental

2.1. Chemicals

Ruthenium chloride (RuCl$_3$, 99+%, ACROS), lithium triethylborohydride (superhydride, Acros Organics, 1 M in THF), 4-aminobiphenyl

* Corresponding author. Fax: +1 831 459 2935.
E-mail address: schen@chemistry.ucsc.edu (S. Chen).

(BPNH$_2$, Aldrich), 4-butylaniline (C4PhNH$_2$, 97%, Sigma Aldrich), 4-hexylaniline (C6PhNH$_2$, 97%, Sigma Aldrich), 4-octylaniline (C8PhNH$_2$, 97%, Sigma Aldrich), 4-decylaniline (C10PhNH$_2$, 97%, Sigma Aldrich), 4-dodecylaniline (C12PhNH$_2$, 97%, Sigma Aldrich), fluoroboric Acid (HBF$_4$, 48–50%, Fisher Chemicals), and sodium nitrite (NaNO$_2$, ARCOS Organics) were all used as received. Solvents were purchased from typical commercial sources at their highest purity and used without further treatment. Water was supplied by a Barnstead Nanopure Water system (18.3 MΩ cm).

2.2. Synthesis of diazonium fluoroborate

The diazonium fluoroborate compounds were synthesized by following a literature protocol [8,9]. Briefly, a calculated amount of the corresponding aniline precursor was dissolved in ice cold 50% fluoroboric acid. Then a 1:1 stoichiometric amount of sodium nitrite was added into the reaction vessel. The solution was allowed to mix for several minutes. The resulting diazonium tetrafluoroborate compound was then washed thoroughly with cold fluoroboric acid and ether, and used immediately in the synthesis of ruthenium nanoparticles.

2.3. Synthesis of ruthenium nanoparticles

The ruthenium nanoparticles were prepared by following an earlier synthetic protocol [2,3]. In a typical synthesis, 0.2 mmol of ruthenium chloride was dissolved in 20 mL of 0.5 M HCl. In a separate reaction vessel, 0.6 mmol of the diazonium tetrafluoroborate salt prepared above was dissolved in 40 mL of toluene. Each solution was stirred for 20 min before the diazonium salt solution was added to the ruthenium chloride solution. The solution was allowed to stir for four more hours so that there was a complete transfer of the ruthenium ions into the toluene phase. The organic phase was collected, to which 10 equivalents of superhydride (~5 mL) were added in a dropwise fashion. The solution color slowly changed from dark red/maroon to black, indicating the formation of ruthenium nanoparticles. After vigorous stirring for two more hours, the nanoparticle solution was washed with 0.5 M H$_2$SO$_4$, 0.5 M Na$_2$CO$_3$, and water to remove inorganic impurities. Excessive free ligands were removed by centrifugation with the addition of ethanol and methanol. The purified products are denoted as follows to reflect the different aliphatic protecting ligands: RuBP (biphenyl), RuPhC4 (butylphenyl), RuPhC6 (hexylphenyl), RuPhC8 (octylphenyl), RuPhC10 (decylphenyl), and RuPhC12 (dodecylphenyl). The ruthenium nanoparticles were found to be soluble in apolar organic solvents such as dichloromethane, toluene, and THF (and remained so after being removed from the solutions, which could be repeated for a number of times – this suggests the formation of a rather compact protecting layer on the particle surface), but insoluble in polar solvents such as ethanol and methanol. Extensive spectroscopic (e.g., UV–Vis, NMR, and FTIR) characterizations were then carried out to verify the complete removal of excessive free ligands before the particles were subject to electrochemical assessment of the electronic conductivity.

2.4. Transmission electron microscopy (TEM)

The particle core diameter and lattice fringes were examined with a Philips CM200/FEG high-resolution transmission electron microscope (HRTEM) operated at 200 keV at the Molecular Foundry/National Center for Electron Microscopy at Lawrence Berkeley National Laboratory. The samples were prepared by casting a drop of the particle solution (~1 mg/mL) in dichloromethane onto a 200-mesh carbon-coated copper grid. The particle core diameter

was estimated by using ImageJ® software analysis of the TEM micrographs.

2.5. Solid-state conductivity

A particle thick film was prepared by dropcasting a concentrated solution (typically 50 mg/mL) of the ruthenium nanoparticles onto the finger region of a gold interdigitated array (IDA) electrode (25 pairs of gold fingers of 3 mm × 5 μm × 5 μm, from ABTECH). The electrode was then placed inside a cryogenic vacuum chamber (Janis Research Co.), and the current–potential (I–V) profiles were collected with a CHI 770 Electrochemical Workstation at varied temperatures which were controlled by a Lakeshore Temperature Controller (Model 311) within the temperature range of 80–300 K. The ensemble conductivity (σ) was evaluated using the equation $\sigma = \frac{1}{49R}\frac{S}{L}$ where R is the ensemble resistance calculated from the slope of the I–V curves, L is the IDA electrode interfinger gap (5 μm), and S is the film cross-section area approximated by (finger height, 5 μm) × (finger length, 3 mm). The constant (49) reflects the 49 junctions which are in parallel within the IDA chip.

3. Results and discussion

Transmission electron microscopy (TEM) has been one of the primary techniques used in the characterization of nanoparticle dimensions, surface morphology, and crystalline structures. Fig. 1 depicts a representative TEM micrograph of the RuPhC6 nanoparticles. It can be seen that the particles are all well dispersed on the Cu grid, where the lack of particle aggregation suggests sufficient protection of the nanoparticle cores by the aliphatic ligands through metal–carbon covalent bonds [2,3]. In addition, the size
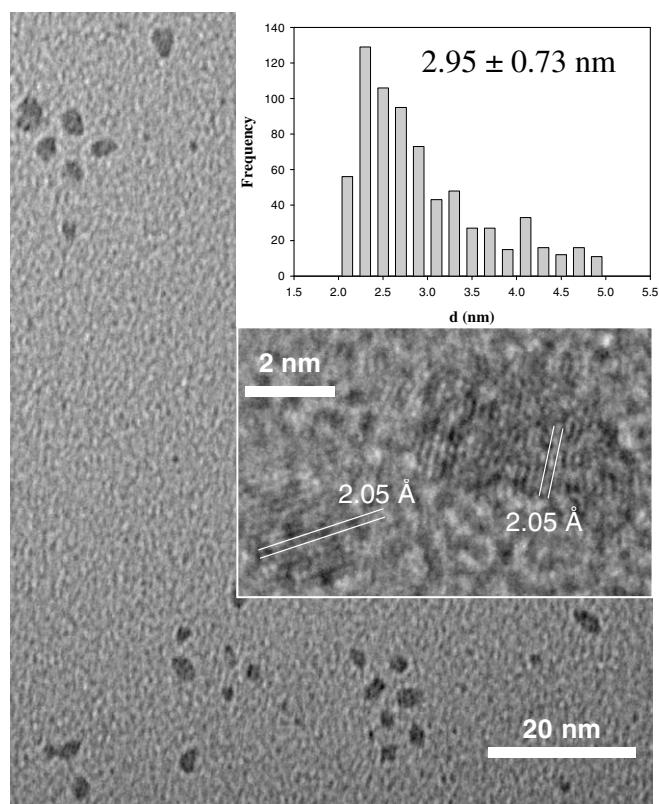

Fig. 1. Representative TEM micrograph of RuPhC6 nanoparticles. A high-resolution TEM micrograph is also shown in the bottom inset where the lattice fringe of 2.05 Å is identified for Ru(1 0 1). The top inset shows the particle core size histogram.

Table 1
Summary of the average core diameter (d) of ruthenium nanoparticle estimated from TEM measurements

Nanoparticle	RuBP	RuPhC4	RuPhC6	RuPhC8	RuPhC10	RuPhC12
d (nm)	3.06 ± 0.84	2.68 ± 0.66	2.95 ± 0.73	3.15 ± 0.70	3.39 ± 0.87	3.22 ± 0.78

of the particles is reasonably monodisperse, with the majority of particles falling within the narrow range of 2–3 nm in diameter, as depicted in the core size histogram (top inset to the figure). In fact, statistical analysis based on measurements of more than seven hundred particles shows that the average particle core diameter is 2.95 ± 0.73 nm. The presence of a ruthenium metal core is further confirmed by high-resolution TEM measurements (bottom inset). It can be seen that lattice fringes of 2.05 Å are clearly resolved, which are ascribed to the Ru(1 0 1) crystalline planes.

Similar TEM profiles were observed with other ruthenium nanoparticles in the series, and the results are summarized in Table 1. Of note is that despite the different chemical structure of the aliphatic ligands, there is little variation of the particle core size (all around 3 nm in dia.) and dispersity (approximately 25%). This may be, at least in part, accounted for by the dynamics of nanoparticle formation which is presumed to be controlled by two competing processes [10], nucleation of the elemental atoms to form the metal cores and passivation of the cores by the binding of protecting ligands. In the present study, the strong Ru–C covalent bond renders the impact of van der Waals interactions between neighboring ligands minimal on particle stabilization.

The nanoparticles obtained above were then subject to extensive spectroscopic characterizations to verify the complete removal of excessive free ligands. For instance, FTIR measurements revealed the disappearance of the vibrational band of the diazonium moiety (N≡N, at *ca.* 2250 cm^{-1}); and in ^{1}H NMR measurements, no sharp features within the range of 7–8 ppm were observed, as the signals of the phenyl protons were broadened into baseline because of their close proximity to the particle cores [2,3]. Both results unambiguously indicate that the particle samples are free of excessive ligands.

Electrochemical evaluation of the particle solid-state conductivity was then carried out. Fig. 2 shows the *I–V* profiles of the series of Ru–C nanoparticles with the temperature varied within the range of 80–300 K. There are at least three aspects that warrant special attention here. First, it can be seen that regardless of the chemical structure of the aliphatic ligands, the *I–V* curves all exhibit a linear (ohmic) profile within the entire temperature range under study, suggesting very efficient interparticle charge transfer. Second, the film conductivity (σ) decreases with increasing temperature (highlighted by arrows in Fig. 2, and further illustrated in panel (A) of Fig. 3), a behavior typically observed with metallic
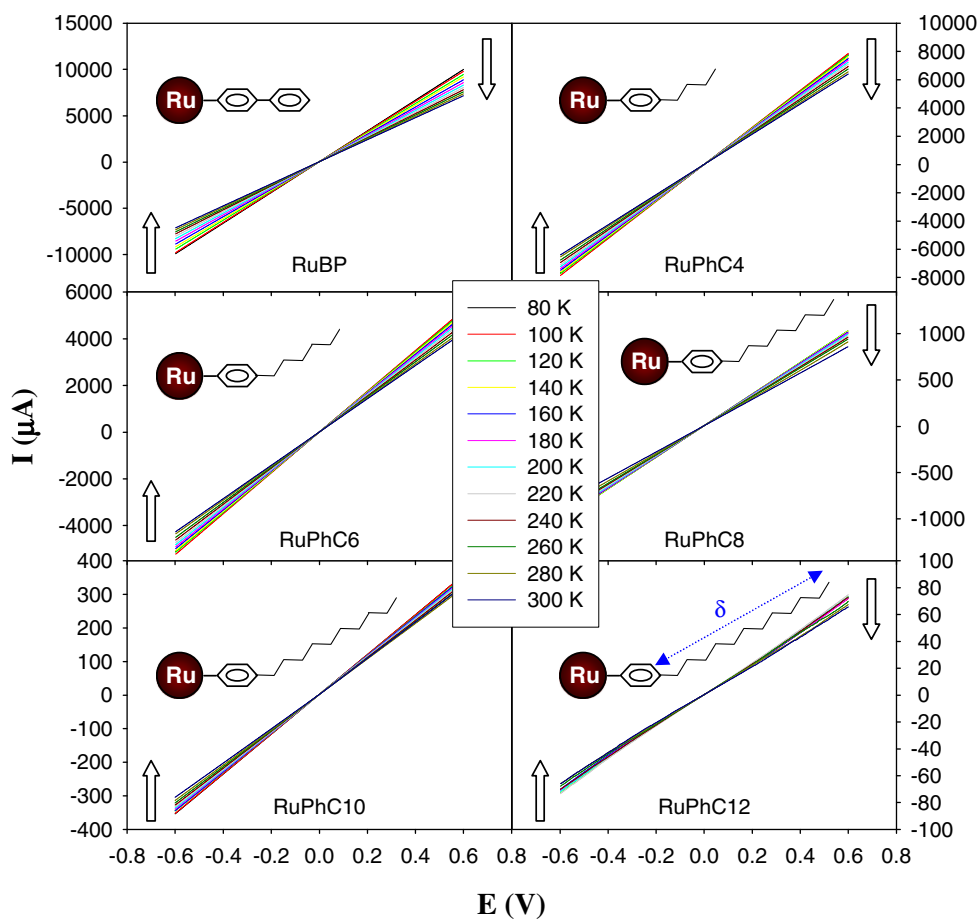

Fig. 2. Current–potential (*I–V*) profiles of solid films of the series of ruthenium nanoparticles at varied temperatures (shown as figure legends). Potential sweep rate 20 mV/s. Arrows signified the decrease of film conductance with temperature. The respective nanoparticle structure was also included in each panel, and the length of the saturated alkyl spacer was denoted as δ.
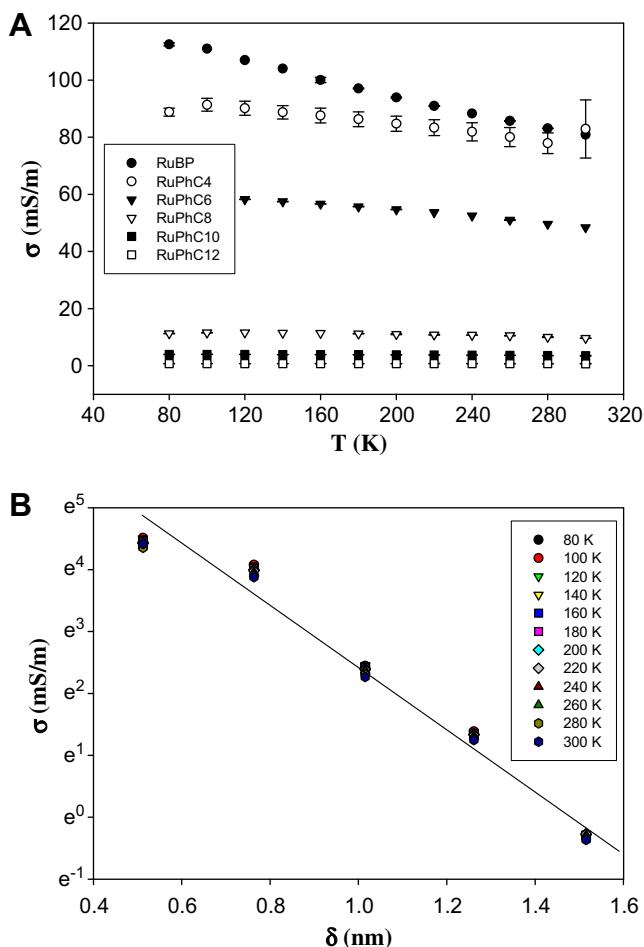
Fig. 3. (A) Temperature dependence of the electronic conductivity of the ruthenium nanoparticles. (B) Variation of the nanoparticle electronic conductivity with the chainlength of the alkyl segment of the particle protecting ligands (δ). Line is linear regression. Error bars are estimated from statistical average of at least three independent measurements.

materials. In previous studies with Pd–C and Ti–C nanoparticles [2,3], the metallic characters are generally observed only with particles passivated with short aliphatic ligands (e.g., biphenyl and butylphenyl). In the present study, such metallic characteristics remain well-defined even with particles protected by relatively long aliphatic ligands such as the decylphenyl and dodecylphenyl fragments. This unusual behavior may be attributed to the significantly stronger Ru–C covalent bond that leads to extended spilling of the core electrons into the organic protecting shell and hence enhanced interparticle charge transfer. In other words, this observation strongly suggests that the ensemble conductivity may be sensitively varied by the metal–ligand interfacial contact.

Third, at any given temperature, the ensemble conductivity decreases with increasing length (δ, Fig. 2) of the saturated alkyl spacer in the particle protecting ligands, which is manifested in panel (B) of Fig. 3. For instance, RuBP nanoparticles exhibited conductivity of the order of 10^2 mS/m, the highest among the series; whereas RuPhC12 nanoparticles were the least conductive, with the conductivity of the order of 1 mS/m. In comparison to pure ruthenium metal (conductivity of 1.4×10^7 S/m) [7], these nanoparticle samples are 8 to 10 orders of magnitude less conductive, as a result of the encapsulation of the metal cores by the insulating organic protecting layer [2,3].

Furthermore, if one assumes that in solid-state, the intercalation of the alkyl segments of the protecting ligands between neighboring particles occurs, the barrier of interparticle charge transfer would be effectively determined by the length of this alkyl spacer (δ), as the phenyl moiety is substantially more conductive [11]. In fact, Fig. 3 (B) depicts an exponential decay of the particle ensemble conductivity with δ within the entire temperature range ($\sigma \propto e^{-\beta \delta}$), with an electronic coupling coefficient (β) of 0.48 Å^{-1}. This is surprisingly low for charge transfer through a saturated alkyl pathway, because such a low value ($\beta = 0.4$–0.5 Å^{-1}) is typically observed with electron transfer through a π-conjugated linker [12,13]. This may be accounted for, again, by the strong metal–ligand covalent bonding interactions that lead to spilling of the core electrons into the organic protecting shells and hence enhanced interparticle charge transfer.

The results were drastically different when the particles were passivated by metal–sulphur bonds. For instance, for gold nanoparticles passivated by alkanethiolates where the alkyl shells serve as the insulating layer for interparticle electron transfer (hopping) [14], the β coefficient estimated from conductivity measurements of the particle solid films is about 1.2 Å^{-1}, which is very close to those measured in electron transfer through rigid alkyl bridges on an electrode surface [15]. A close value of the electronic coupling coefficient ($\beta = 0.8$ Å^{-1}) was also found with arenethiolate-protected gold nanoparticles [11] where the alkyl spacer of the arenethiolate ligands served as the primary barrier for interparticle charge transfer. In these nanoparticle systems, the key structural discrepancy as compared to the Ru–C particles in the present study is the metal–ligand bonding interactions. That is, with the localized Au–S bonds, minimal impact is observed of the core electrons on interparticle charge transfer through the organic protecting matrix.

4. Concluding remarks

Stable ruthenium nanoparticles were synthesized and passivated by metal–carbon covalent bonds. Because of the strong Ru–C bonding interactions, electronic conductivity of the nanoparticle solid films was found to be substantially enhanced as compared to that of particles protected by mercapto-derivatives. Importantly, within the temperature range of 80–300 K, the series of ruthenium nanoparticles exhibited a decrease of the ensemble conductivity with increasing temperature, a characteristic typically observed with metallic materials. Additionally, the ensemble conductivity was found to decay exponentially with the length of the alkyl spacer in the protecting ligands, with the electronic coupling coefficient around 0.48 Å^{-1}, very comparable to that found with charge transfer through a π-conjugated linker. These unique charge-transfer characteristics were attributed to the extended spilling of core electrons into the organic protecting shell that facilitates interparticle charge transfer.

References

[1] G. Schmid, Chem. Rev. 92 (1992) 1709.
[2] D. Ghosh, S.W. Chen, J. Mater. Chem. 18 (2008) 755.
[3] D. Ghosh, S. Pradhan, W. Chen, S.W. Chen, Chem. Mater. 20 (2008) 1248.
[4] W. Chen, J.R. Davies, D. Ghosh, M.C. Tong, J.P. Konopelski, S.W. Chen, Chem. Mater. 18 (2006) 5253.
[5] F. Mirkhalaf, J. Paprotny, D.J. Schiffrin, J. Am. Chem. Soc. 128 (2006) 7400.
[6] W. Chen, S.W. Chen, F.Z. Ding, H.W. Wang, L.E. Brown, J.P. Konopelski, J. Am. Chem. Soc. 130 (2008) 12156.

[7] D.R. Lide, CRC Handbook of Chemistry and Physics: A Ready-Reference Book of Chemical and Physical Data, 85th edn., CRC Press, Boca Raton, 2004.
[8] E.B. Starkey, Org. Synth. 19 (1939) 40.
[9] H.H. Yang, R.L. McCreery, Anal. Chem. 71 (1999) 4081.
[10] S.W. Chen, A.C. Templeton, R.W. Murray, Langmuir 16 (2000) 3543.
[11] W.P. Wuelfing, R.W. Murray, J. Phys. Chem. B 106 (2002) 3139.
[12] S.B. Sachs et al., J. Am. Chem. Soc. 119 (1997) 10563.
[13] S. Creager et al., J. Am. Chem. Soc. 121 (1999) 1059.
[14] R.H. Terrill et al., J. Am. Chem. Soc. 117 (1995) 12537.
[15] R.E. Holmlin et al., J. Am. Chem. Soc. 123 (2001) 5075.